ISSN 1061-933X, Colloid Journal, 2020, Vol. 82, No. 6, pp. 705–712. © Pleiades Publishing, Ltd., 2020.
Russian Text © The Author(s), 2020, published in Kolloidnyi Zhurnal, 2020, Vol. 82, No. 6, pp. 725–732.

Experimental Study of Transport Coefficients of Aqueous Suspensions of Nanodiamonds

M. I. Pryazhnikov[a, b], A. V. Minakov[a, b, *], A. I. Lyamkin[a], V. E. Red'kin[a], S. M. Zharkov[a, c], and G. M. Zeer[a]

[a] *Siberian Federal University, Krasnoyarsk, 660041 Russia*
[b] *Kutateladze Institute of Thermophysics, Siberian Branch, Russian Academy of Sciences, Novosibirsk, 630090 Russia*
[c] *Kirensky Institute of Physics, Federal Research Center "Krasnoyarsk Scientific Center," Siberian Branch, Russian Academy of Sciences, Krasnoyarsk, 660036 Russia*
**e-mail: Aminakov@sfu-kras.ru*

Received August 24, 2018; revised July 2, 2020; accepted July 6, 2020

Abstract—This article presents experimental data on the coefficients of viscosity and thermal and electrical conductivities, as well as the absorption spectra, of suspensions of ultradispersed diamonds. Suspensions of UDA-S and UDP-A detonation nanodiamond particles, as well as UDP-AG diamond–graphite powder, are used in the experiments. The concentration of nanodiamonds in distilled water is varied within a range of 0.5–5 wt %. It is shown that the technology of purification diamond powders from side products of their synthesis substantially affects the physicochemical properties of aqueous suspensions of these powders.

DOI: 10.1134/S1061933X20060101

INTRODUCTION

In 1982–1984, Starver and researchers of the Lavrentiev Institute of Hydrodynamics, Siberia Branch, Russian Academy of Sciences, proposed a method for obtaining ultradispersed diamond–graphite and diamond powders from explosive materials (EMs) containing excess carbon [1, 2]. It is believed that the method for preparing ultradispersed materials from EMs has been studied in detail, and the experimental relations between the main parameters (EM mass and type, chamber volume, gas specific heat, etc.) have been found for optimizing the synthesis process and preserving resulting solid phases [3, 4].

In 1985, the industrial production of ultradispersed diamond–graphite (UDDG) and diamond (UDD) powders was, for the first time, organized at the Research and Production Association "Altai" (Biysk). A great series of scientific, experimental, and technological works was also implemented there for the first time in the field of the development, investigation, and application in industry of technologies and materials using UDDGs and UDDs [3–5].

Somewhat later, joint works in this field were organized under the guidance of Staver at the Department of Physics of Krasnoyarsk Scientific Center, Siberian Branch, Russian Academy of Sciences, and the Scientific Research Laboratory of Ultradispersed Materials of Krasnoyarsk State Technical University. Several production departments were created for the synthesis of ultradispersed diamond–graphite powder of the UDP-AG brand, (Techical Certificate TU 40-2067910-01-91) and diamond powder of the UDP-A brand (Technical Certificate TU 3974-001-10172699-94). Several dozen diverse materials were developed on the basis of UDP-A and UDP-AG powders [5–7]. UDP-A and UDP-AG powders were successfully used as additives to motor and lubricating oils, structural modifiers of rubbers and polymer composites, additives to lacquer and electroplated coatings, quality boosters for aluminum alloys, etc.

The goal of this work was to study diverse physicochemical properties of aqueous suspensions of detonation nanodiamonds produced by different technologies.

EXPERIMENTAL

Diamond powder of the UDA-S brand (TU 84-1124-87) purchased from the Federal Scientific and Production Center FNPTs Altai, UDP-A diamond powder, and UDP-AG diamond–graphite powder were used in the work. The UDP-AG powder is a product of the detonation transformation of organic nitrocompounds; it is represented by a black powder, which consists of the cubic modification of diamond and graphite. In fact, UDP-AG is an initial raw material, the purification of which yields the UDA-S and UDP-A diamond powders.

All suspensions considered in the work were prepared and investigated using the same techniques. The

Table 1. Average sizes and ζ-potentials of particles and pH values of their suspensions

Sample	d_1, nm	d_2, nm	pH	ζ-potential, mV
UDP-AG suspension	55	1010	8.23	+0.42
UDA-S suspension	36	690	5.52	−9.47
UDP-A suspension	28	290	3.07	−21.6

suspensions were obtained by the addition of a required amount of an ultradispersed powder to distilled water followed by mechanical stirring. After that, the suspensions were sonicated for 30 min in a Sapphir TC-10338 ultrasonic bath. Longer sonication caused no changes in the properties of the suspensions. UDP-AG suspensions remained stable with respect to sedimentation for 6–8 h after the sonication, while suspensions of powders of the UDA-S and UDP-A brands were stable for 36–48 h. The measurements showed that, within this period, the physical properties of the suspensions remained unchanged. The stability of the properties of the studied suspensions was controlled primarily by measuring their viscosity. The viscosity of a colloidal system is very sensitive to sedimentation and aggregation of particles. Moreover, the viscosity coefficient is measured quickly and easily. After a time, visible sediments arose in the suspensions. Therefore, to avoid the influence of nanoparticle sedimentation, all experiments were carried out within a few hours after the sonication of the suspensions.

Suspension viscosities were measured using a Brookfield DV2T rheometer equipped with LV-61 and LV-62 spindles and a ULA(0) adaptor for measuring low viscosities. The setup and results of its approbation for measuring the viscosity of nanosuspensions have been described in our previous work [8]. The error in the viscosity measurements was no larger than 2%.

The thermal conductivity coefficients of the suspensions were measured by the procedure developed in our previous work [9]. This procedure is based on the nonstationary hot-wire method [10].

Absorption spectra of the suspensions were recorded using a Genesys 10S Vis spectrophotometer (Thermo Fisher Scientific).

The sizes and electrokinetic (ζ) potentials of the particles in the aqueous suspensions were measured using a DT1200 acoustic/electroacoustic spectrometer (Dispersion Technologies).

The microstructure and phase composition of the powders were studied using a JEM-2100 high-resolution transmission electron microscope (TEM) (JEOL, Japan) equipped with an Oxford Inca x-sight energy-dispersive spectrometer.

Diffraction patterns of the diamond powders were recorded with a Bruker D8 Advance diffractometer (Germany) using Cu$K_{\alpha 1}$ radiation (λ = 1.54056 Å) in a range of scattering angles 2θ from 20° to 85° with a step of 0.05°.

The specific conductance of the suspensions was measured using an ANION 7025 conductometer. The measurements were performed in a conductivity range from 10^{-4} to 10 S/m; the limit of the permissible basic relative error was ±2%.

RESULTS AND DISCUSSION

Average Sizes and ζ-Potentials of the Particles

Table 1 presents the ζ-potentials and sizes of nanoparticles, as well as the pH values of the studied suspensions with a concentration of 5 wt %. The presented data were obtained as the average values of 5 measurements, which were performed at a temperature of 25°C.

The data in Table 1 indicate a significant differences between the properties of the suspensions. The suspension of UDP-AG diamond–graphite particles is slightly alkaline, whereas the suspensions of diamond nanoparticles are acidic. Moreover, the particles have markedly different values of the ζ-potential, the absolute value of which is largest for the particles of the UDP-A suspension. As a consequence, this suspension exhibits a substantially higher stability. This is confirmed by the data on the rate of sediment formation.

Figure 1 shows the particle size distribution density functions measured for 5 wt % suspensions immediately after their preparation. The curves depicted in Fig. 1 show a bimodal particle size distribution. In addition, Table 1 presents the nanoparticle sizes that correspond to the maxima of the bimodal distributions. The diamond–graphite powder suspension contains particles with average sizes of 55 and 1010 nm, the particle sizes in the UDA-S suspension are 37 and 690 nm, and the UDP-A suspension contains particles with sizes of 28 and 290 nm. Thus, the aggregate sizes are smallest in the UDP-A suspension.

Viscosities of the Suspensions

Viscosity is an important property of suspensions from the viewpoint of their practical application. Figure 2 illustrates the dependences of viscosity coefficient μ and yield stress τ on share rate $\dot{\gamma}$ for the studied suspensions with particle concentration C_m = 5 wt %. The behaviors of the viscosity coefficients are markedly different. The viscosity coefficient of the UDP-A suspension is much lower than that of the UDP-AG and UDA-S suspensions at all values of the shear rate. The UDP-AG and UDA-S suspensions have close apparent viscosities. Moreover, as follows from the plots in Fig. 2a, at this nanoparticle concentration, the viscosity depends on the shear rate; hence, these suspensions are non-Newtonian.

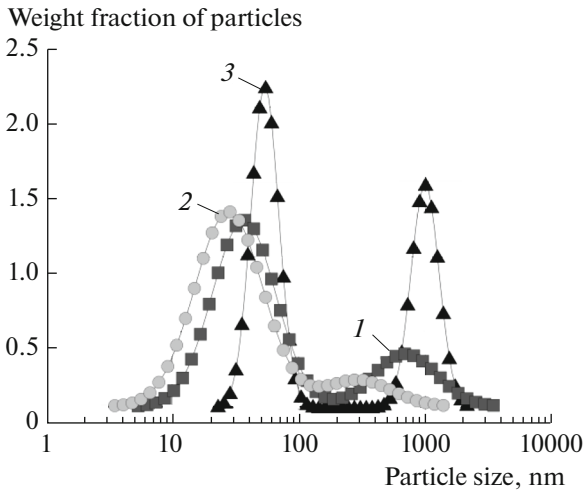

Fig. 1. Particle size distributions in suspensions (*1*) UDA-S, (*2*) UDP-A, and (*3*) UDP-AG.

The rheological behavior of the studied suspensions was, in general, described by the Herschel–Bulkley model:

$$\mu(\dot{\gamma}) = (K\dot{\gamma}^n + \tau_0)/\dot{\gamma},$$

where K is the consistency factor and τ_0 is the yield stress of a viscoplastic fluid. Figure 3 shows the dependences of τ_0, K, and exponent n on the mass concentration of particles. As C_m increases, exponent n decreases, while the value τ_0 increase. A similar rheological behavior was previously observed for other nanosuspensions [11, 12].

The analysis of the results shows that the UDP-AG and UDA-S suspensions exhibit non-Newtonian properties already at a mass concentration of the particles higher than 0.5%. At the same time, the UDP-A suspension remains to be Newtonian at $C_m \le 2.5\%$. Figures 2b and 3a show another important difference between the rheological properties of the studied nanosuspensions. For the UDP-AG and UDA-S suspensions, yield stress τ_0 arises at a particle mass concentration of about 1% and grows with C_m. However, the yield stress of the UDP-A suspension is almost zero even at the maximum concentration. The rheological behavior of the UDP-A suspension is more adequately described by power model $\mu(\dot{\gamma}) = K\dot{\gamma}^{n-1}$.

Thus, at high concentrations, the UDP-AG and UDA-S suspensions are viscoplastic fluids, while the UDP-A suspensions are pseudoplastic ones. The non-Newtonian properties are, most likely, due to the structuring of the suspensions. The tendency of the UDD particles to form a network of aggregates results from a large specific surface area and the existence of a developed functional coating on their surface. The differences in the natures and amounts of the functional groups on the surfaces of the UDP-A and UDA-S particles cause differences in their adsorption properties and aggregation abilities, thereby leading to different rheological behaviors of their suspensions. When studying the stability of aqueous nanodiamond suspensions, Chiganova found that their critical structuring concentration is 0.85 vol % [23, 31]. This value is in good agreement with the results of our measurements of the rheological properties of UDP-A suspensions, for which the onset of non-Newtonian behavior was observed at particle concentrations above 0.8 vol %. Therewith, the non-Newtonian behavior of the UDA-S suspensions began to be observed at much lower volume concentrations of the particles (about 0.2%). The aggregate sizes in the UDA-S suspension are several times larger than those in the UDP-A suspension under the same conditions (see Table 1). Seemingly, it is this fact that leads to the appearance of the non-Newtonian properties of the UDA-S suspension at lower particle concentrations, as compared with the UDP-A suspension.

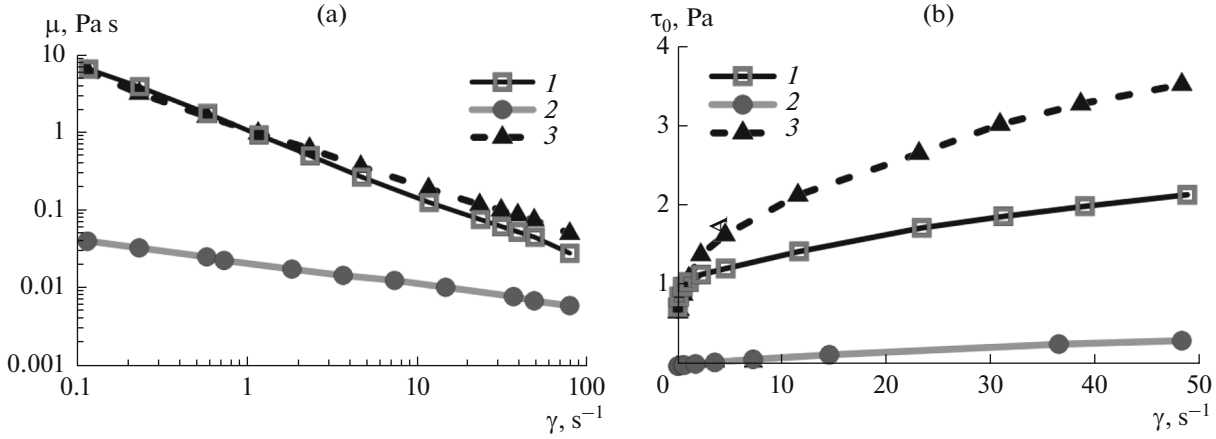

Fig. 2. Dependences of (a) viscosity coefficient and (b) yield stress on shear rate for suspensions (*1*) UDA-S, (*2*) UDP-A, and (*3*) UDP-AG.

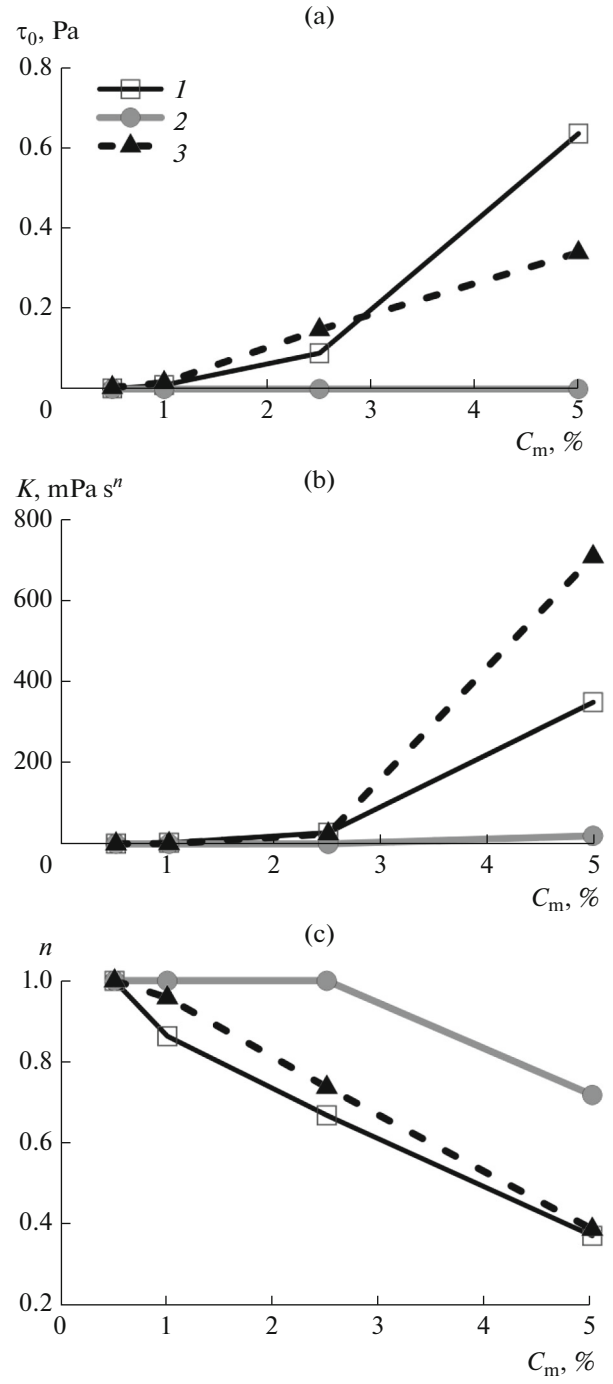

Fig. 3. Dependences of (a) yield stress τ_0, (b) consistency factor K, and (c) exponent n on particle concentration for suspensions (*1*) UDA-S, (*2*) UDP-A, and (*3*) UDP-AG.

The viscosity coefficients obtained for the suspensions (at concentrations at which the viscosity still remains to be Newtonian) were compared with the values calculated by the classical Einstein equation [13]: $\mu = \mu_0(1 + 5/2\,\varphi)$, where φ is the particle volume concentration. For $\varphi = 1.4\%$ ($C_m \approx 2.5\%$), the Einstein equation gives relative viscosity coefficient $\mu/\mu_0 = 1.035$. This value is much lower than the coefficients measured for the studied suspensions ($\mu/\mu_0 = 1.27$ for UDP-A). These data once more confirmed that, in many cases, the classical Einstein theory incorrectly describes the viscosity of nanosuspensions, because it takes into account neither the nanoparticle size nor (all the more) their surface properties [14, 15].

Thermal Conductivities of the Suspensions

Another important property of a suspension is its thermal conductivity. The thermal conductivity of fluids plays a crucial role in the operation of heat-generating equipment. One of the techniques improving the thermal conductivity of fluids is the addition of particles with a high thermal conductivity coefficient to them [16, 17]. In this connection, it is of interest to study the thermal conductivity coefficients of the diamond nanosuspensions.

Figure 4 shows the results of measuring the heat conductivity coefficients for suspensions of nanodiamonds and UDP-AG nanoparticles. Here, the relative thermal conductivity is understood as the ratio between the thermal conductivities of a suspension and water at 25°C. For comparison, the same plot shows the values of thermal conductivity calculated using the Maxwell model [18]:

$$\frac{\lambda}{\lambda_f} = \frac{\lambda_p + 2\lambda_f + 2\varphi(\lambda_p - \lambda_f)}{\lambda_p + 2\lambda_f - \varphi(\lambda_p - \lambda_f)},$$

where λ_p and λ_f are the thermal conductivity coefficients of the particle material and water, respectively. Volume concentration φ may be determined from the following relations: $\rho = \varphi\rho_p + (1 - \varphi)\rho_f$, $\rho C_m = \rho_p\varphi$, where ρ, ρ_p, and ρ_f are the densities of the suspension, particles, and water, respectively.

As follows from Fig. 4, the measured thermal conductivities of the suspensions are adequately described by the classical Maxwell theory. The deviation from the theoretical predictions is within the measurement error. Formally, the largest increment of the thermal conductivity coefficient is observed for the suspension of the UDP-AG diamond–graphite powder.

Absorption Spectra of the Suspensions

Recently, relatively many works have been published devoted to the use of nanosuspensions as working bodies in solar thermal collectors [19, 20]. In contrast to the majority of pure liquids used as heat-transfer agents, nanosuspensions efficiently absorb solar radiation due to the presence of solid particles. In this regard, information on the efficiency of radiation absorption by the studied suspensions is of practical interest. Figure 5 shows the absorption spectra of the

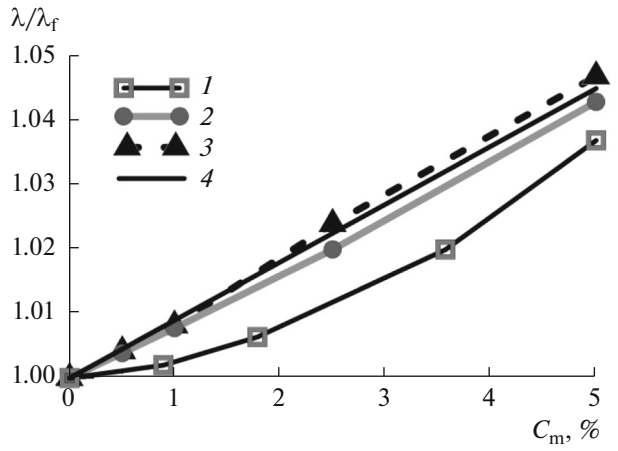

Fig. 4. Dependences of thermal conductivity coefficient on particle concentration for suspensions (*1*) UDA-S, (*2*) UDP-A, and (*3*) UDP-AG; (*4*) calculation by the Maxwell model.

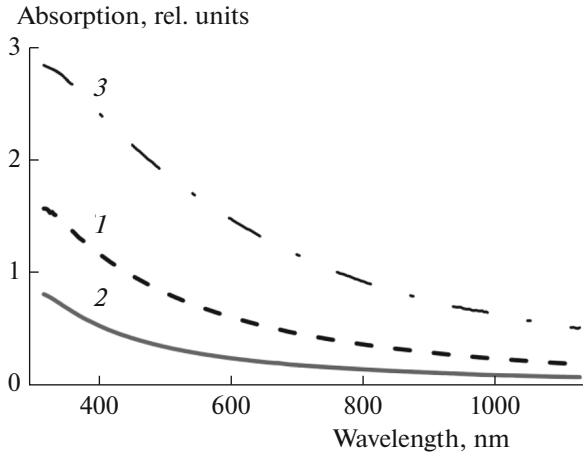

Fig. 5. Absorption spectra of suspensions (*1*) UDA-S, (*2*) UDP-A, and (*3*) UDP-AG.

suspensions. The suspensions of the diamond–graphite powder particles exhibit the highest absorption coefficient within the entire spectral region. In addition, it has been found that the absorption coefficient of the UDA-S suspension is nearly three times higher than that of the UDP-A suspension. Note that UDA-S powder and its suspensions have a much darker color. This is due to different degrees of purification of diamond powders from graphite particles in different production processes.

Electrical Conductivity of the Suspensions

The electrical conductivities of the suspensions were measured with a conductometer (Fig. 6). The suspensions prepared from the diamond–graphite powder and UDP-A particles have exhibited the highest and lowest electrical conductivities, respectively. The dependences of the specific electrical conductivity of the suspensions on the particle concentration are linear: $S = AC_m + B$. Term B is 3.1×10^{-4} S/m. Coefficient A is equal to 148×10^{-4}, 106×10^{-4}, and 379×10^{-4} S/(m wt %) for the UDP-C, UDP-A, and UDP-AG suspensions, respectively.

The data on the electrical conductivity, ζ-potential, pH, and viscosity indicate that the properties of the UDA-S suspension are much closer to those of the suspensions of the diamond–graphite particles. The analysis of literature data have shown that the effective electrical conductivity of diamond nanoparticles is more than an order of magnitude higher than the electrical conductivity values of background electrolytes associated with impurities [21, 22].

It has been shown [21] that the main contribution to the electrical conductivity of the aqueous suspensions of diamond nanoparticles is made by the diffuse part of an electrical double layer, which arises at a diamond particle due to ionization of functional groups on its surface. In the case of nanodiamonds, a charge is, as a rule, generated on the particle surface due to the ionization of the surface functional groups via an acidic or a basic mechanism [23–26].

Transmission Electron Microscopy

The electron microscopic examinations have shown that the UDP-A sample contains diamond nanoparticles with average sizes of 4–8 nm, although particles as large as 15 nm in diameter are sometimes found in the sample (Fig. 7a). The UDA-S sample contains primary nanoparticles with sizes of 4–6 nm (Fig. 7b).

Electron microdiffraction patterns are presented in the inserts of Fig. 7. The diffraction reflections of UDA-S and UDP-A correspond to a cubic diamond

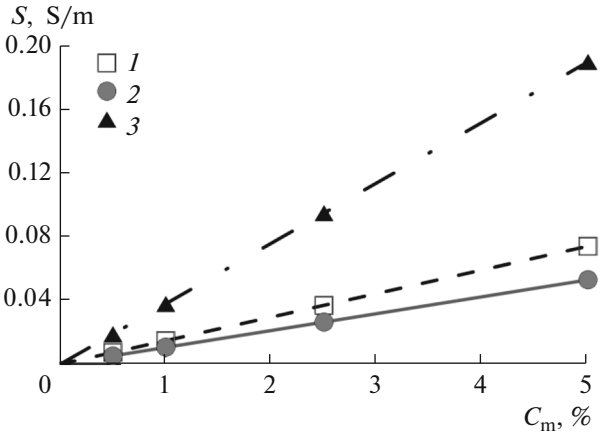

Fig. 6. Concentration dependences of specific electrical conductivity for suspensions (*1*) UDA-C, (*2*) UDP-A, and (*3*) UDP-AG.

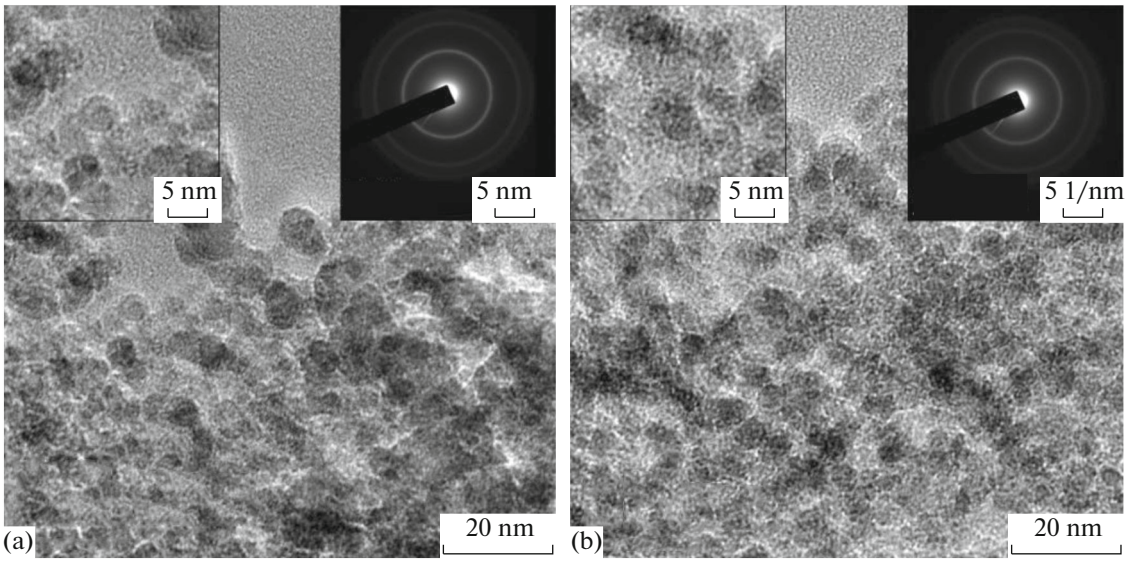

Fig. 7. TEM micrographs of diamond powders (a) UDP-A and (b) UDA-S.

phase (*Fd3m* space group, lattice parameter a = 3.567 Å, PDF 4+ card #00-006-0675 [27]).

The electron microscopic investigations of UDP-AG diamond–graphite powder (Fig. 8) have revealed that the small particles are represented by nanodiamonds and graphite nanoparticles. In addition to nanodiamonds and graphite nanoparticles, the sample contains almost spherical particles with sizes of 30 nm to 0.5 μm. These particles contain iron in concentrations as high as 40 wt % (Fig. 8b, Table 2). Pure carbon "rods" with lengths of 10 μm and above are also observed (Fig. 8b, Tabl. 2).

X-ray Diffraction Analysis of the Powders

The analysis of the diamond powders (Fig. 9) has revealed that the peaks in the X-ray diffraction patterns correspond to the diamond phase. For example, at $2\theta \approx 44.3°$, the lattice parameter is equal to 2.07042 and 2.06635 Å for UDA-S and UDP-A particles, respectively. At $2\theta \approx 76.3°$, these values are 1.26079 and 1.26370 Å, respectively. As follows from [27], the interplanar distances for diamond are: d (111) = 2.060 Å and d (220) =1.261 Å. In addition to the peaks corresponding to the diamond phase, the X-ray diffraction patterns of the diamond–graphite powder contain peaks due to graphite, magnetite Fe_3O_4, and hematite Fe_2O_3.

Table 2. Quantitative relations of elements (%) at selected points of the UDP-AG sample (see Fig. 8b)

Spectrum number	C	O	Fe	Total
Spectrum 1	60.24	16.66	23.10	100.00
Spectrum 2	58.12	15.84	26.03	100.00
Spectrum 3	45.54	14.87	39.59	100.00
Spectrum 4	31.32	68.68	–	100.00

CONCLUSIONS

The article reports the experimental data on the properties of aqueous suspensions of UDA-S and UDP-A ultradispersed diamonds and UDP-AG diamond–graphite powder, with particle concentrations of 0.5–5 wt %. The viscosity, thermal conductivity, and electrical conductivity coefficients and the pH values of the suspensions, as well as the ζ-potentials of the particles have been measured. The particle size distributions and the absorption spectra of the suspensions have been determined.

The data on the electrical conductivity, ζ-potential, pH, and viscosity have shown that the properties of the UDA-S suspension are much closer to the properties of the diamond–graphite suspension than those of the UDP-A suspension. The significant differences revealed in the properties of the studied suspensions are due to different technologies of purification of the initial diamond–graphite powder from nondiamond components.

Previous investigations [28–31] showed that the methods for purification of nanodiamonds from impurities were crucial for the composition of functional groups formed on their surface. Ultradispersed diamonds obtained from the products of their synthesis using boric anhydride (UDP-A) have a higher oxygen content (up to 15 vs. 9% for UDA-S) and a significant amount of boron (2.3%) [31]. The doping with boron gives rise to additional useful properties of UDP-A, such as the increased resistance of the powder to caking and the stability of its aqueous suspen-

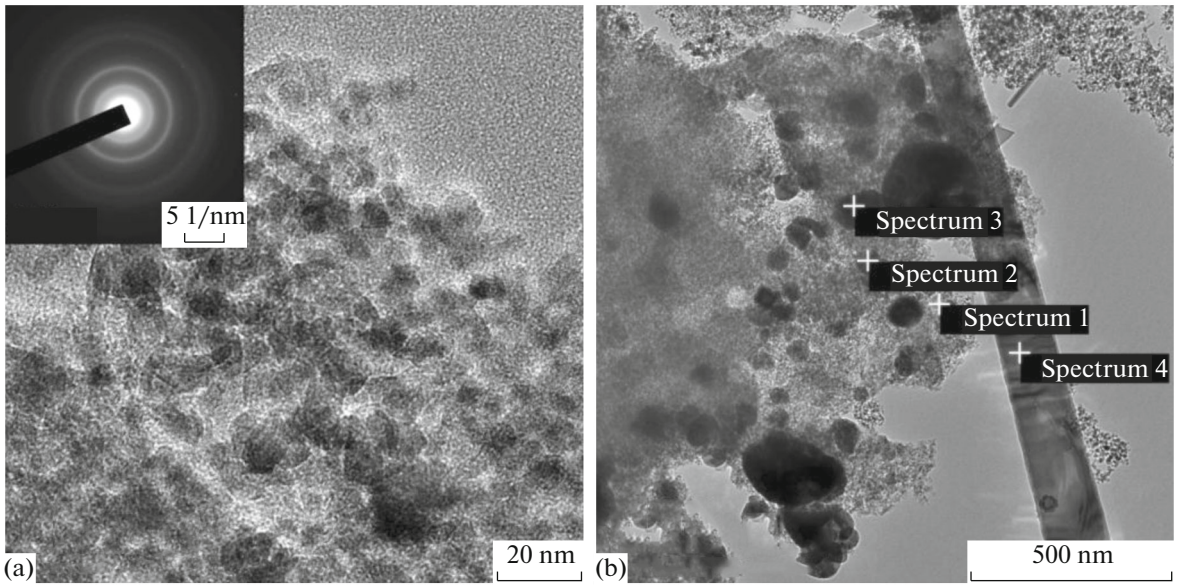

Fig. 8. TEM micrographs taken from diamond–graphite powder at different magnifications: (a) ×150000 and (b) ×15000. Crosses indicate the points, at which spectra 1–4 were recorded to determine the elemental composition.

sion. The purification of UDA-S with a mixture of sulfuric and nitric acids increases the contents of nitrogen and sulfur. In addition, the examination of the surface has shown the presence of hydrocarbon fragments (methyl and aromatic groups) and oxygen-containing ones (carbonyl, carboxyl, and hydroxyl groups). Therewith, the analysis of the surface functional groups [31] has revealed that the fraction of strongly acidic functional groups in UDA-S is smaller (about 30% of the total content) than that in UDP-A (as large as 60%).

The influence of UDD purification method on the composition of the functional groups is due to a high fraction of surface atoms and the formation of chemical bonds with substances used in the purification process. The conditions of nondiamond carbon phase oxidation also affect the oxygen content in the functional coating of the particles. Therefore, the method of purifying UDDs significantly affects the physicochemical properties of the prepared suspensions.

The results obtained in the work may be useful for the application of nanodiamond suspensions in various fields (medicine, heat transfer intensification, electrochemistry, electrodeposition, tribology, additives to lubricants, etc.).

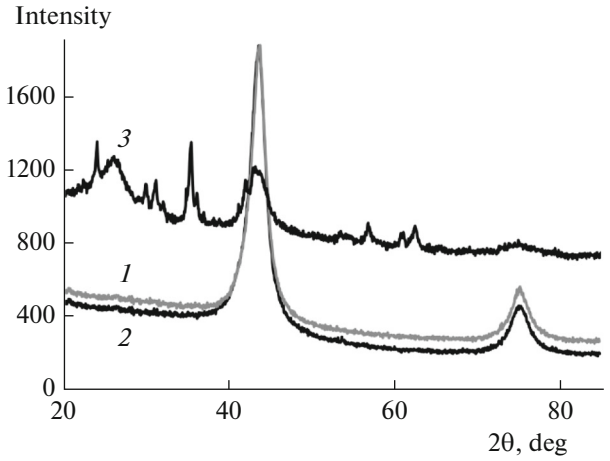

Fig. 9. X-ray diffraction patterns of powders (*1*) UDA-S, (*2*) UDP-A, and (*3*) UDP-AG.

CONFLICT OF INTEREST

The authors declare that they have no conflicts of interest.

FUNDING

This work was carried out within the framework of the state order of the Ministry of Science and Higher Education of the Russian Federation (project no. FSRZ-2020-0012).

REFERENCES

1. Staver, A.M., Gubareva, N.V., Lyamkin, A.I., and Petrov, E.A., USSR Inventor's Certificate no. 1165007, 1982.
2. Lyamkin, A.I., Petrov, E.A., Ershov, A.P., Sakovich, G.V., Staver, A.M., and Titov, V.M., *Dokl. Akad. Nauk SSSR*, 1988, vol. 302, p. 611.
3. Staver, A.M., Gubareva, N.V., Lyamkin, A.I., and Petrov, E.A., *Fiz. Goreniya Vzryva*, 1984, no. 5, p. 100.

4. Sakovich, G.V., Komarov, V.F., and Petrov, E.A., *Sverkhtverd. Mater.*, 2002, no. 3, p. 3.
5. Chiganova, G.A and Chiganov, A.S., *Russ. J. Appl. Chem.*, 1998, vol. 71, p. 1832.
6. Red'kin, V.E. and Mishin, A.A., *Reshetnevskie Chteniya*, 2011, vol. 1, p. 403.
7. Sakovich, G.V., Zharkov, A.S., and Petrov, E.A., *Nanotechnol. Russ.*, 2013, vol. 8, nos. 9–10, p. 581.
8. Rudyak, V.Ya., Minakov, A.V., Smetanina, M.S., and Pryazhnikov, M.I., *Dokl. Akad. Nauk*, 2016, vol. 467, p. 289.
9. Minakov, A.V., Rudyak, V.Ya., Guzei, D.V., Pryazhnikov, M.I., and Lobasov, A.S., *Inzh.-Fiz. Zh.*, 2015, vol. 88, p. 148.
10. Platunov, E.S., Baranov, I.V., Buravoi, S.E., and Kurepin, V.V., *Teplofizicheskie izmereniya: uchebnoe posobie* (Thermophysical Measurements: A Manual), Platunov, E.S., Ed., St. Petersburg: SPbGUNiPT, 2010.
11. Minakov, A.V., Rudyak, V.Y., and Pryazhnikov, M.I., *Colloids Surf. A*, 2018, vol. 554, p. 279.
12. Sharma, A.K., Tiwari, A.K., and Dixit, A.R., *Renew. Sust. Energ. Rev.*, 2016, vol. 53, p. 779.
13. Batchelor, G.K., *J. Fluid Mech.*, 1977, vol. 83, p. 97.
14. Puzyr', A.P., Minakov, A.V., Burov, A.E., Zharkov, S.M., Maksimov, N.G., and Pryazhnikov, M.I., *Colloid J.*, 2017, vol. 79, p. 258.
15. Rudyak, V.Ya. and Minakov, A.V., *Eur. Phys. J. E*, 2018, vol. 41, p. 15.
16. Keblinski, P., Eastman, J.A., and Cahill, D.G., *Mater. Today*, 2005, vol. 8, no. 6, p. 36.
17. Pryazhnikov, M.I., Minakov, A.V., Rudyak, V.Ya., and Guzei, D.V., *Int. J. Heat Mass Transfer*, 2017, vol. 104, p. 1275.
18. Hamilton, R.L. and Crosser, O.K., *Ind. Eng. Chem. Fundam.*, 1962, vol. 1, p. 187.
19. Leong, K.Y., Ong, H.C., Amer, N.H., Norazrina, M.J., Risby, M.S., and Ku, Ahmad K.Z., *Renew. Sust. Energ. Rev.*, 2016, vol. 53, p. 1092.
20. Bellos, E. and Tzivanidis, C., *J. Therm. Anal. Calorim.*, 2019, vol. 135, p. 763.
21. Zhukov, A.N., Gareeva, F.R., and Aleksenskii, A.E., *Colloid J.*, 2012, vol. 74, p. 463.
22. Shvidchenko, A.V., Zhukov, A.N., Dideikin, A.T., Baidakova, M.V., Shestakov, M.S., Shnitov, V.V., and Vul', A.Ya., *Colloid J.*, 2016, vol. 78, p. 235.
23. Chiganova, G.A., *Colloid J.*, 2000, vol. 62, p. 238.
24. Gibson, N., Shenderova, O., Luo, T.J.M., Moseenkov, S., Bondar, V., Puzyr, A., Purtov, K., Fitzgerald, Z., and Brenner, D.W., *Diam. Relat. Mater.*, 2009, vol. 18, p. 620.
25. Maier, F., Riedel, M., Mantel, B., Ristein, J., and Ley, L., *Phys. Rev. Lett.*, 2000, vol. 85, p. 3472.
26. Chakrapani, V., Angus, J.C., Anderson, A.B., Wolter, S.D., Stoner, B.R., and Sumanasekera, G.U., Science (Washington, D. C.), 2007, vol. 318, p. 1424.
27. www.icdd.com/products/PDF-4+, 2014.
28. Dolmatov, V.Yu., *Usp. Khim.*, 2001, vol. 70, p. 687.
29. Jiang, T. and Xu, K., *Carbon*, 1995, vol. 33, p. 1663.
30. Koshcheev, A.P., *Ross. Khim. Zh.*, 2008, vol. 52, no. 5, p. 88.
31. Chiganova, G.A., *Kolloidn. Zh.*, 1994, vol. 56, p. 266.

Translated by E. Khozina